ACS EARTH AND SPACE CHEMISTRY

http://pubs.acs.org/journal/aesccq

Article

Coesite Formation at Low Pressure during Supersonic Microprojectile Impact of Opal

Seungyeol Lee, Jizhe Cai, Shiyun Jin, Dongzhou Zhang, Ramathasan Thevamaran, and Huifang Xu*

Cite This: *ACS Earth Space Chem.* 2020, 4, 1291−1297

Read Online

ACCESS | Metrics & More | Article Recommendations | Supporting Information

ABSTRACT: The shock metamorphism of opal-A induced by supersonic microprojectile impacts in an advanced laser-induced projectile impact test (LIPIT) was investigated using synchrotron X-ray diffraction (XRD) and transmission electron microscopy (TEM). The three-dimensional topography of the impact area is similar to the meteorite crater that has a circular outline with an uplifted rim. The post-impact synchrotron XRD and TEM analyses show the phase transformation of opal-A to coesite together with opal-CT, tridymite, and cristobalite. The impact simulation estimates that the shocked areas experienced pressures up to ∼0.6−0.7 GPa. The results suggest that the transition pressure from opal-A to coesite is lower than the transition pressure of quartz to coesite (∼2 GPa). The impact-induced phase transformation of opal-A to coesite at low pressure could be related to the local precursor structure (coesite domain) and water content (∼6.7 wt %) in opal-A. The investigation of minerals via the LIPIT technique provides a new way of simple and cost-effective shock-metamorphic experiments. The combined micron-scale ballistic test, impact simulation, and high-resolution characterization techniques will be useful to study the shock metamorphism of various minerals from macro-, micro-, to nanoscale, which will help understand the impact phenomena on Earth, Mars, and many other types of meteorites and asteroids.

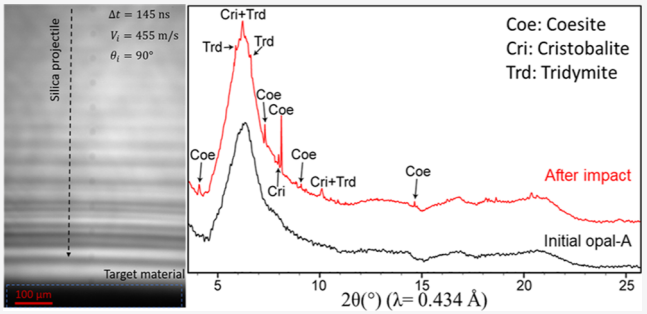

KEYWORDS: *shock metamorphism, opal-A, coesite, LIPIT, XRD, TEM*

1. INTRODUCTION

Shock metamorphism, also called impact metamorphism, is the progressive breakdown and deformation of underlying rock layers and their constituent minerals during an impact event.[1−3] It is caused by intense shock waves creating dynamic pressure and heat that originate at the point of impact, which occurs in natural impacts, nuclear explosions, and cratering experiments.[4−6] Natural shock metamorphism is the physical consequence of meteorite impacts on planetary bodies, leading to the circular or craterlike geological structures, deformed bedrock and sediment, large igneous provinces, economic deposits, and biological extinction events.[7−11] The shock-metamorphic signatures are widely observed in impact craters on Earth, lunar rocks, meteorites, and many other types of asteroids.[1,12−16] On the Earth, impact craters are often heavily eroded; therefore, the shock-metamorphic minerals remain as an explicit indicator for impact event as well as quantitative evidence on the impact pressures and temperatures.[1,6,17] Consequently, shocked minerals represent the most important and unequivocal evidence of terrestrial impact record (e.g., coesite and stishovite in Barringer Meteor Crater of Arizona, Ries Crater of Germany, shocked quartz in Triassic−Jurassic boundary in Italy).[3,18−20]

During a shock event, minerals rapidly adjust to the changing conditions, which can lead to phase transformations, planar defect formation, mechanical twinning, and decomposition.[2,3,6,21] The shock-metamorphic behavior of minerals fundamentally depends on their composition and crystal structure.[1,22] For example, quartz, made of silica tetrahedra (SiO_4) covalently bonded with the three-dimensional network, cannot provide dislocation glide during shock loading, whereas the high density of dislocations can be generated in shocked olivine due to the weak interconnection in isolated silica tetrahedra.[23] Shock metamorphism in rock-forming minerals have been studied since first recognized in the 1960s using optical microscopy and X-ray diffraction (XRD) techniques; however, there is still a lack of the experimental data of shock metamorphism to understand the natural impact phenomena.[1,2,21,24,25] Specifically, it is difficult to acquire experimental data for the behavior of minerals in natural impacts due to the

Received: April 8, 2020
Revised: June 23, 2020
Accepted: July 1, 2020
Published: July 1, 2020

https://dx.doi.org/10.1021/acsearthspacechem.0c00090
ACS Earth Space Chem. 2020, 4, 1291−1297

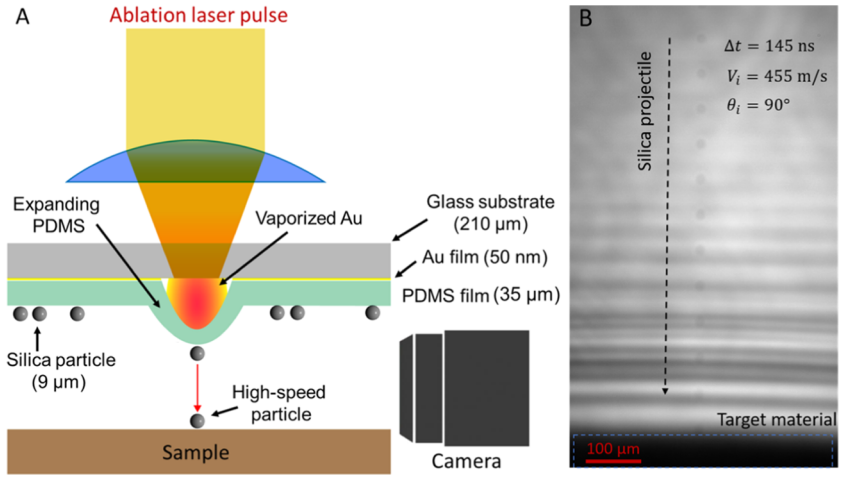

Figure 1. Single silica microprojectile impact experiments. (A) Illustration of the laser-induced single projectile impact experiment. (B) Multiexposure image of silica projectile in flight imaged at 103 ns intervals following laser ablation.

extreme pressures, the post-shock temperature that occurs in just a few seconds during the impact, and the uncertainties in forecasting the impact event.[1,21]

Here, we report an experimental shock metamorphism of opal-A induced by supersonic microprojectile impacts using an advanced laser-induced projectile impact test (LIPIT). The microscopic ballistic technique has previously been used to study dynamic deformation and specific penetration energy of protective nanomaterials as well as to study a martensitic phase transformation in single-crystal metals.[26−31] Opal-A is a hydrated amorphous silica species and a widespread mineraloid on Earth's crust that occurs in vesicles, veins, and fissures of many rocks (e.g., commonly found with sandstone, chalk deposits, limonite, and rhyolite).[32−35] On Mars, the Compact Reconnaissance Imaging Spectrometer for Mars (CRISM) instrument suggests the presence of opaline silica deposits on the Martian surface.[36] In this study, we report the first impact experiments on opal-A. The phase transformation and deformation features of shocked opal-A were investigated by synchrotron XRD and transmission electron microscopy (TEM) analyses. The results of this study provide important information on the shock metamorphism of opal-A from macro to nanoscales.

2. SAMPLES AND METHODS

The opal-A (hyalite opal) sample is from the Chalice mine, North Carolina, showing the globular and botryoidal shape of amorphous silica with glasslike appearance (Supporting Figure S1). The hyalite opal is also called opal-AN, Muller's glass, or jalite. It shows a strong green fluorescence under UV light. Opal-A shows the strain-induced birefringence and wavy textures under the polarized light. The polished thin section of opal-A (~50 μm) is prepared for the impact experiment (Supporting Figure S1). XRD pattern and chemical composition from an electron probe microanalyzer (EPMA) and TEM−energy-dispersive X-ray spectroscopy (EDS) of opal-A are given in Supporting Figures S2 and S3 and Supporting Table S1. The EPMA results show that opal-A consist of SiO_2 (88.24−90.75 wt %), Al_2O_3 (1.73−1.79 wt %), Fe_2O_3 (0.01−0.12 wt %), MgO (0.04−0.06 wt %), CaO (0.36−0.39 wt %), Na_2O (0.05−0.18 wt %), K_2O (0.08−0.13 wt %), and H_2O (6.14−7.25 wt %) (Supporting Table S1). H_2O is calculated by analyzing O using EPMA and assigning the excessive O to H_2O. In nature, hyalite opal typically contains about 3−8 wt % water.[37]

To study the shock metamorphism of opal-A, we used the microballistic technique illustrated in Figure 1. An ablation laser pulse (8−10 ns pulse duration, 1064 nm) from a Nd:YAG laser (Quanta-Ray INDI-40-10-HG, Spectra-Physics) was focused on a launchpad containing spherical silica microprojectiles to selectively propel them at supersonic velocities. The launchpad consists of a poly(dimethylsiloxane) (PDMS) layer (Sylgard 184, Dow Chemical) that was mixed at a ratio of 10:1, spin-coated on a 50 nm thick gold-coated microscope cover glass (210 μm), followed by cured at 100 °C for 1 h. The thickness of the cured PDMS film is approximately 35 μm. Monodisperse amorphous silica microspheres (~9 μm in diameter) were drop-casted on the launchpad, and individual/clusters of microspheres were brought to the focal point of the laser facilitated by an inverted microscope (Figure 1A). Individual and clusters of silica microspheres were selectively launched using an ablation laser pulse that ablates the thin gold film and rapidly expands the PDMS layer, toward the sample at high velocities (~400−500 m/s). The launching velocity of a projectile depends on the characteristics of projectile, launchpad structure, and ablation laser energy, whose mechanism is discussed in a recent publication based on the same LIPIT system.[31] For the launchpad we use, the laser energy is tuned to be at about 100 μJ/pulse using an attenuator to launch the 9.2 μm silica sphere at ~400−500 m/s. The projectile in flight was imaged using an ultrafast multiexposure imaging technique with a high-resolution microscope camera (Allied Vision Mako G-234B with OPTEM FUSION 12.5:1 lens) illuminated by externally shuttered picosecond laser pulses from a supercontinuum white laser (NKT photonics EXR-20) (Figure 1B).

The three-dimensional (3D) topographical features of impact areas were studied by a surface mapping interferometer (Zygo NewView 6300) scanning a white-light interferometer in the Materials Science Center at the University of Wisconsin−Madison. Lab-XRD data were collected with a two-dimensional (2-D) image-plate detector and 0.3 mm beam collimator using a Rigaku Rapid II instrument (Mo Kα radiation) in the Department of Geoscience at the University of Wisconsin−Madison. Wavelength-dispersive spectroscopy (WDS) EPMA measurements were made with a CAMECA

https://dx.doi.org/10.1021/acsearthspacechem.0c00090
ACS Earth Space Chem. 2020, 4, 1291−1297

SXFiveFe electron microprobe using 20 kV in the Department of Geoscience at the University of Wisconsin−Madison. The bright-field and high-resolution TEM images with the selected-area electron diffraction (SAED) were carried out using a Philips CM200-UT transmission microscope operated at 200 kV in the Materials Science Center at the University of Wisconsin−Madison. TEM samples were prepared by depositing a suspension of crushed grains precisely selected from the impact area on a lacy carbon-coated Cu grid. The chemical composition was obtained using X-ray energy-dispersive spectroscopy (EDS) with a Li-drifted Si detector.

Synchrotron radiation X-ray diffraction of shock-impacted opal-A was carried out at the beamline 13-BM-C at the Advanced Photon Source (APS), Argonne National Laboratory. The X-ray beam was monochromated to 28.6 keV (0.434 Å), with a 1 eV bandwidth, and was focused to 12 μm × 18 μm with a Kirkpatrick−Baez mirror. The Pilatus3 1 M detector (Dectris) was placed 170 mm away from the sample, and the NIST standard LaB_6 powder was used to calibrate the distance and tilting of the detector. The sample from the impact area was placed on a silica glass capillary aligned using an optical microscope.

3. RESULTS

The topographical features of craters can provide valuable information on impact processes including physical and geological processes.[37] The 3D topography of impact areas in our opal-A samples is similar to craters formed by meteorite impact, showing a circular outline with the uplifted rim as well as a depth that is shallow relative to the diameter.[38] In addition, the type of multiple craters produced by two projectiles that simultaneously impacted the sample is shown in Figure 2D,E. The impact velocity of the silica projectile and its angle of impact with respect to the surface normal direction were measured using the multiple-exposure images (Figure 2C,F). The silica projectiles were accelerated to velocities in the range of 408−478 m/s (Figure 2C,F). The rebound velocity of a projectile measures ∼324 m/s in Figure 2C.

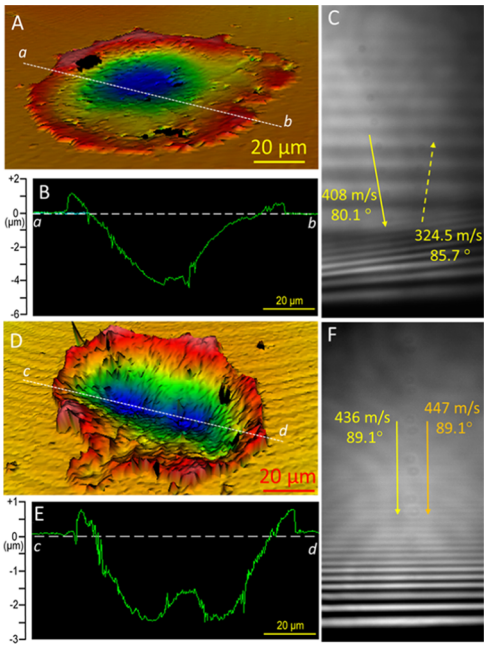

Figure 2. Three-dimensional topography of impact areas of opal-A including the multiexposure image of the respective projectiles in flight. The Zygo 3D optical profilometer was used for characterizing the topography of single impacts (A, B) and double impacts (D, E). A multiexposure image of colliding and rebounding silica projectile with 103 ns intervals after a laser ablation pulse (C, F).

Spatially resolved micro-XRD patterns from the same area before and after the impact were obtained using an in-house X-ray diffractometer (Supporting Figure S1). High-quality spatially resolved micro-XRD patterns were collected from the impacted area of opal-A and an area nearby the microcrater using synchrotron radiation (Figure 3). The diffraction pattern indicates the phase transformation of coesite, cristobalite, and tridymite from opal-A (Figure 3). No quartz was observed in the impacted opal. Coesite is a high-pressure silica (SiO_2) polymorph that is generally formed by meteorite impact or ultra-high-pressure metamorphism (see a phase diagram in Supporting Figure S4).[39,40] Tridymite and cristobalite are high-temperature and low-pressure polymorphs of silica (Supporting Figure S4), but they can also form in a metastable state in low-temperature environments coexisting with opal phases (e.g., hydrothermal fluid).[41] We tested the shock metamorphism of single-crystal quartz and novaculite (microcrystalline quartz) under the same impact condition, but the phase transformation was not observed.

The combination of TEM images with selected-area electron diffraction (SAED) patterns and TEM−EDS spectra was used to identify the minerals.[42,43] The TEM images of initial opal-A show amorphous-like morphology with one broad diffraction ring corresponding to ∼4.0 Å in the SAED pattern (Figure 4A,B). The TEM−EDS analysis of opal-A indicates the presence of minor amounts of Na, Mg, Al, and Ca (Supporting Figure S3). We identified opal-CT, coesite, tridymite, and cristobalite from the shocked opal-A (Figure 4C−F). Figure 4C shows the transformation of the initial opal-A to the opal-CT. TEM images of opal-CT show the nanosized crystals randomly oriented in the matrix with a sharp 4.1-Å diffraction ring in its SAED pattern (Figure 4C). The direct contacts of opal-CT with tridymite, coesite, and cristobalite are observed (Figure 4D−F). The TEM images and SAED pattern of coesite indicate the (100)-twinned $C2/c$ coesite and existence of displacement/stacking faults following $(10\bar{1})$ plane (Figure 4E). Two types of twins with (100) and (021) as twin planes commonly occur in coesite and the (100)-twin corresponds to an operation of a 180° orientation along c-axis like Carlsbad twin in sanidine.[39,40] The structure models of (100)-twinned coesite and displacement along $(10\bar{1})$ plane are illustrated in Supporting Figure S5.

4. IMPACT PRESSURE AND TEMPERATURE

During the impact of microprojectile, the most extreme pressure and heating conditions always happen within the material region directly ahead of the projectile.[29,44] The pressure during initial impact period near this region is approximately calculated using the Rankine−Hugoniot relation, that is derived from conservation of momentum, $P = \rho_0 U_s U_p$, where P, ρ_0, U_s, and U_p are the pressure, initial density, shock wave velocity, and particle velocity in the opal rock sample. The equation of state, which relates the shock velocity to the particle velocity, is $U_s = C_0 + SU_p$, where S is an experimentally determined parameter.

Considering the pressure equilibrium, $P_1 = P_2$ between the projectile (P_1) and target materials (P_2) and assuming the same material properties for a projectile (silica) and target

https://dx.doi.org/10.1021/acsearthspacechem.0c00090
ACS Earth Space Chem. 2020, 4, 1291−1297

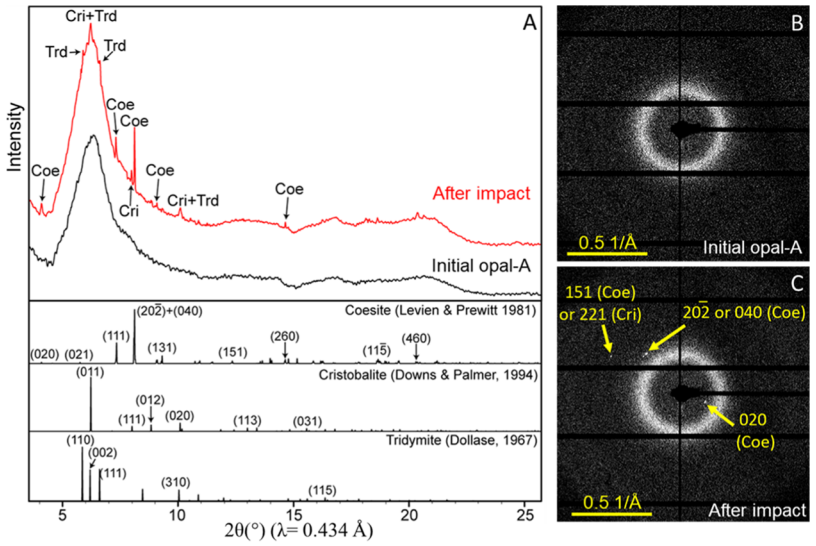

Figure 3. (A) Synchrotron radiation XRD pattern of the impacted opal-A, compared with references coesite (Levien and Prewitt, 1981),[62] cristobalite (Downs and Palmer, 1994),[63] and tridymite (Dollase, 1976).[64] The shocked opal shows the diffraction peaks of coesite (Coe), cristobalite (Cri), and tridymite (Trd). A slice of 2-D image plate showing diffraction ring of initial opal (B) and the diffraction spots from coesite and cristobalite of and the shocked opal (C).

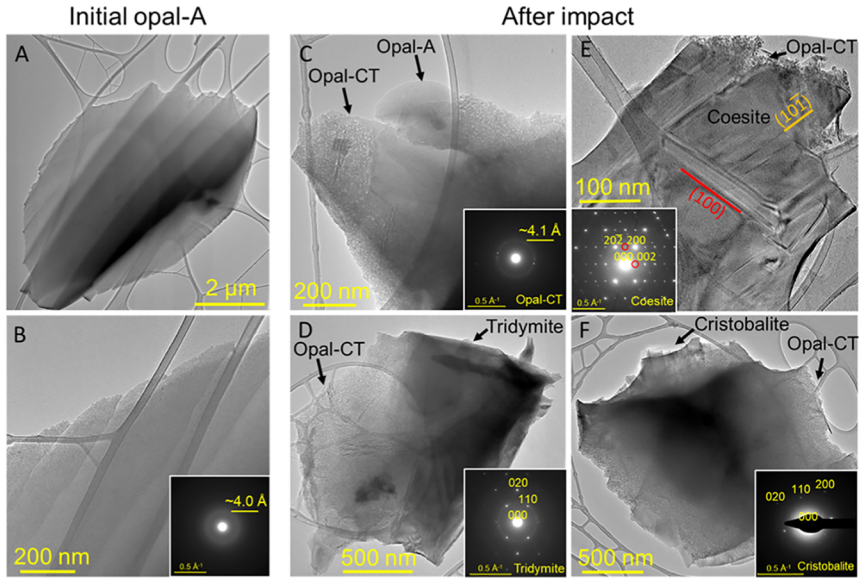

Figure 4. Bright-field TEM images and SAED patterns of initial opal-A (A, B) and impacted opal (C–F). The impacted phase show intergrowth of opal-A and opal-CT and phase transformation products of tridymite, coesite, and cristobalite together with opal-CT. The coesite shows the existence of displacement along $(10\bar{1})$ planes and (100) twin boundary. The weak extra spots in SAED pattern (red circles) may result from interface areas that violate *c*-glide in *C*2/*c* symmetry.

material (amorphous silica glass), the particles' velocities on either side of the impact interface are calculated to be equal, $U_{p1} = U_{p2}$ (Supporting Figure S2). For continuity, $V = U_{p1} + U_{p2}$, where V is the impact speed of the projectile, the particle velocity in the target material will be obtained. Then, the pressure within the opal is obtained with $C_0 = 0.95$ km/s and $S = 1.66$, from experimental results for amorphous silica glass.[45] The pressure within the material with the impact speed from 300 to 500 m/s is shown in Supporting Figure S6. For the impact speed of 400–450 m/s, the pressure generated ahead of projectiles is ~0.6–0.7 GPa (Supporting Figure S6). The temperature rising is estimated to range from 73.4 to 100.8 K during impact (see supplementary text in the Supporting Information).

5. DISCUSSION

The opal is deposited at a relatively low temperature and is found in soils, sediments, and rocks of all continents.[32,33,37] Clarke et al. reported that most soils contain opal-like phases up to 2–3%, which play an essential nutrient to many plants and animals.[35] Hydrated amorphous silica (i.e., opal) has also been identified in abundance on the surface of Mars and meteorites, where it has been formed as a product of aqueous alteration of silicate minerals.[46−50] Opal comprises a significant part of the silica component of continental crusts and astromaterials. It is an important mineral that may experience the natural shock metamorphism. There are no detailed reports of shock-metamorphic experiments on opal-A previously. This might be related to the difficulty of

https://dx.doi.org/10.1021/acsearthspacechem.0c00090
ACS Earth Space Chem. 2020, 4, 1291−1297

characterization of the short-range ordered structure of opal-A.[41,51,52]

A combined method of synchrotron XRD and TEM shows the phase transformation of opal-A to opal-CT, tridymite, cristobalite, and coesite that was induced by the micro-projectile impacts (Figures 3 and 4). The normal shock estimations—an upper bound for the pressure generated by spherical projectiles—suggest that the shocked areas experienced pressures up to ∼0.6−0.7 GPa, which is lower than the pressure of the phase transition boundary (>2 GPa) between α-quartz and coesite (Supporting Figure S4). The impact experiments of single-crystal quartz and novaculite (microcrystalline quartz) do not show other silica polymorphs. Only the impact surface of opal-A shows opal-CT, tridymite, cristobalite, and coesite, which suggests that the crystalline silica phases were transformed from opal-A during the shock metamorphism.

The formation of coesite from opal-A and silica gel has been reported by other studies.[53,54] The coesite was synthesized from opal-A at 700 °C and 3.2 GPa with an end-loaded piston-cylinder apparatus for 95 h duration.[53] The annealing experiment of silica gel containing chlorophyll aggregates resulted in coesite at a temperature of ∼565 °C under an ambient pressure condition, which is also much lower than the coesite field in the phase diagram.[54] A plausible hypothesis for this opal-A to coesite transition at low pressures and temperatures could be associated with opal structure. Martínez et al. suggested that the direct transformation from silica gel to coesite at low-pressure conditions and temperatures is associated with the presence of four-membered SiO_4 rings in the structure of silica gel.[54] Lee reported that opal-A structure mainly consisted of four-membered and six-membered rings of SiO_4 tetrahedra based on pair distribution function study (Supporting Figure S7).[55] The four-membered ring of SiO_4 (i.e., local structure of coesite) could be the precursor to the formation of the microcrystalline coesite, whereas the six-membered rings could be the precursor to the formation of tridymite (two-layer stacking of the SiO_4 tetrahedra ring) and cristobalite (three-layer stacking). In nature, some opal coexisted with low tridymite and low cristobalite without quartz in low-temperature environments.[33,51,55,56]

The presence of water in opal could also have contributed to lower the phase transition pressures. The opal is hydrated amorphous silica ($SiO_2{\cdot}nH_2O$), and this sample contains ∼6.7 wt % water (Supporting Table S1). Previous experiments reported that dry quartz exhibits a high yield strength to fail in the deformation even under pressures of 2−3 GPa.[3,55] On the contrary, wet quartz, containing ∼400 ppm of water, displays plastic behavior and deformations around 0.5−0.6 GPa.[57] Due to the hydrolytic weakening effect and diffusion of water-related point defects, the water in opal could lower the transition boundary.[57,58] Similarly, porous sandstone can form a coesite phase at relatively low shock pressure.[12]

In addition, the TEM image shows the phase transition from opal-A to opal-CT (Figure 4C). In sedimentary rock, opal-A changes to opal-CT during diagenesis.[59,60] The mineralogical transition of opal-A to opal-CT caused changes in rock properties such as porosity, permeability, and acoustic response, which is important to oil and gas exploration to estimate the formation of diagenetic hydrocarbon traps.[60] Several studies have documented that the pressure and temperature are prime determinants of the transition from opal-A (<45 °C) to opal-CT (>160 °C).[32,60] In the shock-metamorphic experiment, the pressure and temperature induced by the impact event cause the transformation of opal-A to opal-CT. The TEM images show that the opal-CT always coexisted with and next to the crystalline phases (i.e., tridymite, cristobalite, and coesite) (Figure 4), which might be related to the intermediate phase as the opal-CT transformed from opal-A during phase transformation or caused by the locally different pressure and temperature distributions.[61]

6. CONCLUSIONS

The investigation of the minerals via high-velocity micro-projectile impacts using the LIPIT technique provides a new way to explore shock metamorphism. Synchrotron XRD and TEM techniques reveal nano- and microscaled phases in the shocked opal-A. The results show the phase transformation of opal-A to coesite, opal-CT, tridymite, and cristobalite at the shocked area, where experienced pressures up to ∼0.6−0.7 GPa. The transition pressure from opal-A to coesite is much lower than the transition pressure of quartz to coesite (∼2 GPa). The phase transition of opal-A to coesite at low pressure could mainly be related to its local structure (coesite domain) and the presence of water in opal-A.

The main advantage of the LIPIT technique is that the size of the projectile and the impact speed can be controlled in desired ways and provides dynamic experiments at length scales that enable a holistic analysis of impact phenomena using electron microscopy and synchrotron X-ray diffraction techniques. The method can be applied to other rock-forming mineral systems in various experimental conditions to mimic collision environments in the laboratory through adjusting the density, speed, and temperature of the projectiles. Furthermore, the shock-metamorphic experiments can be used to study the specific orientations of minerals that respond to impact along with different incident directions. Various dynamic effects originating from time, angle, grain size, and thickness can systematically be studied to provide a detailed understanding of shock metamorphism and impact-induced structural transformations in rock-forming minerals. In summary, the integrated LIPIT microprojectile experiments and post-impact electron microscopy and synchrotron characterization methods along with potential computational modeling will benefit the study of shock metamorphism in minerals and lead to expanding our knowledge of shock metamorphism on Earth, Moon, Mars, and other planetary bodies.

■ ASSOCIATED CONTENT

Supporting Information

The Supporting Information is available free of charge at https://pubs.acs.org/doi/10.1021/acsearthspacechem.0c00090.

Optical images of opal-A (Figure S1); lab-XRD patterns of opal-A and projectiles (Figure S2); TEM−EDS spectra of opal-A (Figure S3); phase diagram of silica polymorphs (Figure S4); structure models of planar defects (Figure S5); impact pressure estimates of shocked opal-A (Figure S6); PDF patterns of opal-A and silica polymorphs (Figure S7); major element composition of opal-A via EPMA analysis (Table S1); and the supplementary text for estimation of average temperature rise due to the impact (PDF)

https://dx.doi.org/10.1021/acsearthspacechem.0c00090
ACS Earth Space Chem. 2020, 4, 1291−1297

AUTHOR INFORMATION

Corresponding Author

Huifang Xu − *Department of Geoscience, University of Wisconsin−Madison, Madison, Wisconsin 53706, United States;* orcid.org/0000-0002-7464-0057; Phone: 1-608-265-5887; Email: hfxu@geology.wisc.edu

Authors

Seungyeol Lee − *Department of Geoscience, University of Wisconsin−Madison, Madison, Wisconsin 53706, United States; USRA Lunar and Planetary Institute, Houston, Texas 77058, United States; ARES, NASA Johnson Space Center, Houston, Texas 77058, United States;* orcid.org/0000-0002-0175-1389

Jizhe Cai − *Department of Engineering Physics, University of Wisconsin−Madison, Madison, Wisconsin 53706, United States;* orcid.org/0000-0003-2803-2111

Shiyun Jin − *Department of Geoscience, University of Wisconsin−Madison, Madison, Wisconsin 53706, United States*

Dongzhou Zhang − *Hawaii Institute of Geophysics and Planetology, University of Hawaii at Manoa, Honolulu, Hawaii 96822, United States; GeoSoilEnviroCARS, University of Chicago, Lemont, Illinois 60439, United States*

Ramathasan Thevamaran − *Department of Engineering Physics, University of Wisconsin−Madison, Madison, Wisconsin 53706, United States;* orcid.org/0000-0001-5058-6167

Complete contact information is available at: https://pubs.acs.org/10.1021/acsearthspacechem.0c00090

Notes

The authors declare no competing financial interest.

ACKNOWLEDGMENTS

The authors acknowledge NASA Astrobiology Institute (NNA13AA94A) for supporting this study. Part of this work was performed at GeoSoilEnviroCARS (Sector 13), Partnership for Extreme Crystallography program (PX^2), Advanced Photon Source (APS), and Argonne National Laboratory. GeoSoilEnviroCARS is supported by the National Science Foundation—Earth Sciences (EAR-1634415) and Department of Energy—Geosciences (DE-FG02-94ER14466). PX^2 program is supported by COMPRES under NSF Cooperative Agreement EAR-1661511.

REFERENCES

(1) Langenhorst, F.; Deutsch, A. Shock metamorphism of minerals. *Elements* **2012**, *8*, 31−36.

(2) French, B. M. Shock metamorphism of natural materials. *Science* **1966**, *153*, 903−906.

(3) Stöffler, D.; Langenhorst, F. Shock metamorphism of quartz in nature and experiment: I. Basic observation and theory. *Meteoritics* **1994**, *29*, 155−181.

(4) Short, N. M. Progressive shock metamorphism of quartzite ejecta from the Sedan nuclear explosion crater. *J. Geol.* **1970**, *78*, 705−732.

(5) Fink, J.; Greeley, R.; Gault, D. In *Impact Cratering Experiments in Bingham Materials and the Morphology of Craters on Mars and Ganymede*, Lunar and Planetary Science Conference, 1982; Vol. *12*, pp 1649−1666.

(6) Langenhorst, F. Shock metamorphism of some minerals: Basic introduction and microstructural observations. *Bull. Czech Geol. Surv.* **2002**, *77*, 265−282.

(7) French, B. M.; Koeberl, C. The convincing identification of terrestrial meteorite impact structures: What works, what doesn't, and why. *Earth-Sci. Rev.* **2010**, *98*, 123−170.

(8) Ganapathy, R. A major meteorite impact on the earth 65 million years ago: Evidence from the Cretaceous-Tertiary boundary clay. *Science* **1980**, *209*, 921−923.

(9) Kyte, F. T.; Zhou, L.; Lowe, D. R. Noble metal abundances in an Early Archean impact deposit. *Geochim. Cosmochim. Acta* **1992**, *56*, 1365−1372.

(10) Jones, A. P. Meteorite impacts as triggers to large igneous provinces. *Elements* **2005**, *1*, 277−281.

(11) French, B. M. Sudbury structure, Ontario: Some petrographic evidence for origin by meteorite impact. *Science* **1967**, *156*, 1094−1098.

(12) Kieffer, S. W. Shock metamorphism of the Coconino sandstone at Meteor Crater, Arizona. *J. Geophys. Res.* **1971**, *76*, 5449−5473.

(13) Von Engelhardt, W.; Arndt, J.; Müller, W.; Stöffler, D. Shock metamorphism of lunar rocks and origin of the regolith at the Apollo 11 landing site. *Geochim. Cosmochim. Acta Suppl.* **1970**, *1*, 363−384.

(14) Bischoff, A.; Stöffler, D. Shock metamorphism as a fundamental process in the evolution of planetary bodies: Information from meteorites. *Eur. J. Mineral.* **1992**, *4*, 707−755.

(15) Stöffler, D.; Keil, K.; Scott, E. R. D. Shock metamorphism of ordinary chondrites. *Geochim. Cosmochim. Acta* **1991**, *55*, 3845−3867.

(16) Rubin, A. E. Postshock annealing and postannealing shock in equilibrated ordinary chondrites: Implications for the thermal and shock histories of chondritic asteroids. *Geochim. Cosmochim. Acta* **2004**, *68*, 673−689.

(17) Grieve, R. A.; Langenhorst, F.; Stöffler, D. Shock metamorphism of quartz in nature and experiment: II. Significance in geoscience. *Meteorit. Planet. Sci.* **1996**, *31*, 6−35.

(18) Bice, D. M.; Newton, C. R.; McCauley, S.; Reiners, P. W.; McRoberts, C. Shocked quartz at the Triassic-Jurassic boundary in Italy. *Science* **1992**, *255*, 443−446.

(19) Grieve, R.; Sharpton, V.; Stöffler, D. Shocked minerals and the K/T controversy. *Trans., Am. Geophys. Union* **1990**, *71*, 1792.

(20) Fahey, J. Recovery of coesite and stishovite from Coconino sandstone of Meteor Crater, Arizona. *Am. Mineral.* **1964**, *49*, 1643−1647.

(21) Stöffler, D.; Hamann, C.; Metzler, K. Shock metamorphism of planetary silicate rocks and sediments: Proposal for an updated classification system. *Meteorit. Planet. Sci.* **2018**, *53*, 5−49.

(22) Leroux, H. Microstructural shock signatures of major minerals in meteorites. *Eur. J. Mineral.* **2001**, *13*, 253−272.

(23) Langenhorst, F.; Boustie, M.; Migault, A.; Romain, J. Laser shock experiments with nanoseconds pulses: a new tool for the reproduction of shock defects in olivine. *Earth Planet. Sci. Lett.* **1999**, *173*, 333−342.

(24) Bunch, T.; Cohen, A. J. Coesite and shocked quartz from Holleford crater, Ontario, Canada. *Science* **1963**, *142*, 379−381.

(25) Chao, E.; Fahey, J.; Littler, J.; Milton, D. Stishovite, SiO_2, a very high pressure new mineral from Meteor Crater, Arizona. *J. Geophys. Res.* **1962**, *67*, 419−421.

(26) Thevamaran, R.; Lawal, O.; Yazdi, S.; Jeon, S. J.; Lee, J. H.; Thomas, E. L. Dynamic creation and evolution of gradient nanostructure in single-crystal metallic microcubes. *Science* **2016**, *354*, 312−316.

(27) Xie, W.; Alizadeh-Dehkharghani, A.; Chen, Q.; Champagne, V. K.; Wang, X.; Nardi, A. T.; Kooi, S.; Müftü, S.; Lee, J. H. Dynamics and extreme plasticity of metallic microparticles in supersonic collisions. *Sci. Rep.* **2017**, *7*, No. 5073.

(28) Xue, S.; Fan, Z.; Lawal, O. B.; Thevamaran, R.; Li, Q.; Liu, Y.; Yu, K.; Wang, J.; Thomas, E. L.; Wang, H. High-velocity projectile impact induced 9R phase in ultrafine-grained aluminium. *Nat. Commun.* **2017**, *8*, No. 1653.

(29) Lee, J. H.; Veysset, D.; Singer, J. P.; Retsch, M.; Saini, G.; Pezeril, T.; Nelson, K. A.; Thomas, E. L. High strain rate deformation of layered nanocomposites. *Nat. Commun.* **2012**, *3*, No. 1164.

(30) Lee, J. H.; Loya, P. E.; Lou, J.; Thomas, E. L. Dynamic mechanical behavior of multilayer graphene via supersonic projectile penetration. *Science* **2014**, *346*, 1092−1096.

(31) Cai, J.; Thevamaran, R. Superior Energy Dissipation by Ultrathin Semicrystalline Polymer Films Under Supersonic Microprojectile Impacts. *Nano Lett.* **2020**, DOI: 10.1021/acs.nanolett.0c00066.
(32) Curtis, N. J.; Gascooke, J. R.; Johnson, M. R.; Pring, A. A Review of the Classification of Opal with Reference to Recent New Localities. *Minerals* **2019**, *9*, No. 299.
(33) Jones, J. B.; Segnit, E. R. The nature of opal I. Nomenclature and constituent phases. *J. Geol. Soc. Aust.* **1971**, *18*, 57−68.
(34) Liesegang, M.; Milke, R. Australian sedimentary opal-A and its associated minerals: Implications for natural silica sphere formation. *Am. Mineral.* **2014**, *99*, 1488−1499.
(35) Clarke, J. The occurrence and significance of biogenic opal in the regolith. *Earth-Sci. Rev.* **2003**, *60*, 175−194.
(36) Milliken, R. E.; Swayze, G. A.; Arvidson, R. E.; Bishop, J. L.; Clark, R. N.; Ehlmann, B. L.; Green, R. O.; Grotzinger, J. P.; Morris, R.; Murchie, S. L.; et al. Opaline silica in young deposits on Mars. *Geology* **2008**, *36*, 847−850.
(37) Graetsch, H. Structural Characteristics of Opaline and Microcrystalline Silica Minerals. In *Silica*, Heaney, P. J., Prewitt, C. T., Gibbs, G. V., Eds.; Mineralogical Society of America: Washington, DC, 1994; Vol. *29*, pp 209−232.
(38) Head, J. W., III; Fassett, C. I.; Kadish, S. J.; Smith, D. E.; Zuber, M. T.; Neumann, G. A.; Mazarico, E. Global distribution of large lunar craters: Implications for resurfacing and impactor populations. *Science* **2010**, *329*, 1504−1507.
(39) Chao, E. C.; Shoemaker, E. M.; Madsen, B. M. First natural occurrence of coesite. *Science* **1960**, *132*, 220−222.
(40) Massonne, H.-J. First find of coesite in the ultrahigh-pressure metamorphic area of the central Erzgebirge, Germany. *Eur. J. Mineral.* **2001**, *13*, 565−570.
(41) Lee, S.; Xu, H.; Xu, W.; Sun, X. The structure and crystal chemistry of vernadite in ferromanganese crusts. *Acta Crystallogr., Sect. B: Struct. Sci., Cryst. Eng. Mater.* **2019**, *75*, 591−598.
(42) Lee, S.; Xu, H.; Xu, H.; Jacobs, R.; Morgan, D. Valleyite: A new magnetic mineral with the sodalite-type structure. *Am. Mineral.* **2019**, *104*, 1238−1245.
(43) Xu, H.; Lee, S.; Xu, H. Luogufengite: A new nano-mineral of Fe_2O_3 polymorph with giant coercive field. *Am. Mineral.* **2017**, *102*, 711−719.
(44) Shockey, D. A.; Simons, J. W.; Curran, D. R. The Damage Mechanism Route to Better Armor Materials. *Int. J. Appl. Ceram. Technol.* **2010**, *7*, 566−573.
(45) Alexander, C. S.; Chhabildas, L. C.; Reinhart, W. D.; Templeton, D. W. Changes to the shock response of fused quartz due to glass modification. *Int. J. Impact Eng.* **2008**, *35*, 1376−1385.
(46) Downes, H.; Beard, A.; Franchi, I.; Greenwood, R. In *Origin of Opal (Hydrated Silica) in Polymict Ureilites*, Lunar and Planetary Science Conference, 2016; Vol. *47*, p 1443.
(47) White, J. S., Jr.; Henderson, E.; Mason, B. Secondary minerals produced by weathering of the Wolf Creek meteorite. *Am. Mineral.* **1967**, *52*, 1190−1197.
(48) Rice, M.; Bell, J., III; Cloutis, E.; Wang, A.; Ruff, S.; Craig, M.; Bailey, D.; Johnson, J.; de Souza, P., Jr.; Farrand, W. Silica-rich deposits and hydrated minerals at Gusev Crater, Mars: Vis-NIR spectral characterization and regional mapping. *Icarus* **2010**, *205*, 375−395.
(49) Tosca, N. J.; Knoll, A. H. Juvenile chemical sediments and the long term persistence of water at the surface of Mars. *Earth Planet. Sci. Lett.* **2009**, *286*, 379−386.
(50) McAdam, A. C.; Zolotov, M. Y.; Mironenko, M. V.; Sharp, T. G. Formation of silica by low-temperature acid alteration of Martian rocks: Physical-chemical constraints. *J. Geophys. Res.* **2008**, *113*, No. E08003.
(51) Lee, S.; Xu, H. Using Complementary Methods of Synchrotron Radiation Powder Diffraction and Pair Distribution Function to Refine Crystal Structures with High Quality Parameters—A Review. *Minerals* **2020**, *10*, No. 124.
(52) Lee, S. Investigation of Nanominerals in Geological Systems Using X-Ray, Neutron, and Electron Beams. Ph.D. Dissertation, Univeristy of Wisconsin Madison: Madison, WI, 2019.
(53) Michalski, J. R.; Kraft, M. D.; Diedrich, T.; Sharp, T. G.; Christensen, P. R. Thermal emission spectroscopy of the silica polymorphs and considerations for remote sensing of Mars. *Geophys. Res. Lett* **2003**, *30*, 1−4.
(54) Martínez, J. R.; Vázquez-Durán, A.; Martínez-Castañón, G.; Ortega-Zarzosa, G.; Palomares-Sánchez, S. A.; Ruiz, F. Coesite formation at ambient pressure and low temperatures. *Adv. Mater. Sci. Eng.* **2008**, *2008*, No. 406067.
(55) Lee, S.; Xu, H. Using powder XRD and pair distribution function to determine anisotropic atomic displacement parameters of orthorhombic tridymite and tetragonal cristobalite. *Acta Crystallogr., Sect. B: Struct. Sci., Cryst. Eng. Mater.* **2019**, *75*, 160−167.
(56) Elzea, J. M.; Rice, S. B. TEM and X-ray diffraction evidence for cristobalite and tridymite stacking sequences in opal. *Clays Clay Miner.* **1996**, *44*, 492−500.
(57) Doukhan, J.-C.; Trépied, L. Plastic deformation of quartz single crystals. *Bull. Mineral.* **1985**, *108*, 97−123.
(58) Griggs, D. T.; Blacic, J. D. Quartz: anomalous weakness of synthetic crystals. *Science* **1965**, *147*, 292−295.
(59) Kastner, M.; Keene, J.; Gieskes, J. Diagenesis of siliceous oozes—I. Chemical controls on the rate of opal-A to opal-CT transformation—an experimental study. *Geochim. Cosmochim. Acta* **1977**, *41*, 1041−1059.
(60) Lynne, B. Y.; Campbell, K. A. Morphologic and mineralogic transitions from opal-A to opal-CT in low-temperature siliceous sinter diagenesis, Taupo volcanic zone, New Zealand. *J. Sediment. Res.* **2004**, *74*, 561−579.
(61) Tsuji, T.; Masui, Y.; Yokoi, S. New hydrocarbon trap models for the diagenetic transformation of opal-CT to quartz in Neogene siliceous rocks. *AAPG Bull.* **2011**, *95*, 449−477.
(62) Levien, L.; Prewitt, C. T. High-pressure crystal structure and compressibility of coesite. *Am. Mineral.* **1981**, *66*, 324−333.
(63) Downs, R. T.; Palmer, D. C. The pressure behavior of α-cristobalite. *Am. Mineral.* **1994**, *79*, 9−14.
(64) Dollase, W. The superstructure of meteoritic low tridymite solved by computer simulation. *Am. Mineral.* **1976**, *61*, 971−978.

https://dx.doi.org/10.1021/acsearthspacechem.0c00090
ACS Earth Space Chem. 2020, 4, 1291−1297